Available online at www.sciencedirect.com
SCIENCE DIRECT®
International Journal of Heat and Mass Transfer 48 (2005) 4467–4473
International Journal of HEAT and MASS TRANSFER
www.elsevier.com/locate/ijhmt

Experiments and a model of turbulent exchange flow in a vertical pipe

Murali R. Cholemari, Jaywant H. Arakeri *

Department of Mechanical Engineering, Indian Institute of Science, Bangalore 560012, India

Received 27 December 2004; received in revised form 6 April 2005
Available online 19 July 2005

Abstract

In this paper we present experimental measurements of buoyancy driven turbulent exchange flow in a vertical pipe (L/d ratios of 9–12). The flow is driven by an unstable density difference across the ends of the pipe, created using brine and distilled water. Away from either end, a fully developed region of turbulence exists with a linear density gradient. Using a mixing length model that accounts for the end effects, we obtain the turbulent scales and flux. The Nusselt number scales like the square root of the Rayleigh number ($Nu \sim Ra^{1/2}$). We give an empirical relation to quantify the end effects and hence calculate the flux of the salt (NaCl) given the aspect ratio of the pipe and the overall density difference across it.
© 2005 Elsevier Ltd. All rights reserved.

Keywords: Turbulent mixing; Exchange flow; Mixing length model

1. Introduction

This paper is concerned with turbulent natural convection in a long vertical pipe subject to an unstable density difference across the two ends. In the present paper we model the main mechanism that drives the turbulent flow, validate the model with experimental measurements and extend it to general cases. We discuss the implications of the model on the behaviour of the flux described in terms of a Nusselt number.

Fig. 1 shows the schematic of the flow. The pipe is connected by two tanks, with the top tank fluid having higher density than the bottom tank fluid. The two fluids are miscible. The incompressibility of the fluids implies that the cross section average of the axial velocity at any instant was zero. This type of flow—where the net flow is zero—is termed 'exchange flow' [1,2].

Most of the earlier work on exchange flow [1,2] has been in the context of the fire safety of buildings. Two types of studies have been done of flow through vent(s) connecting two enclosures, one above the other. One is flow due to the combined action of pressure and density differences across the vent, for example, as discussed in Tan and Jaluria [2], and the other type is due to density difference alone, for example as studied in Epstein [1]. The present flow is related to the latter type. Epstein [1] experimentally studied the buoyancy driven exchange (counter-current) flow through single or multiple openings with both square and circular cross sections in horizontal partitions, using brine above the partition and fresh water below the partition. The openings were tubes,

* Corresponding author. Tel.: +91 80 293 3228; fax: +91 80 360 0648.
E-mail address: jaywant@mecheng.iisc.ernet.in (J.H. Arakeri).

0017-9310/$ - see front matter © 2005 Elsevier Ltd. All rights reserved.
doi:10.1016/j.ijheatmasstransfer.2005.04.025

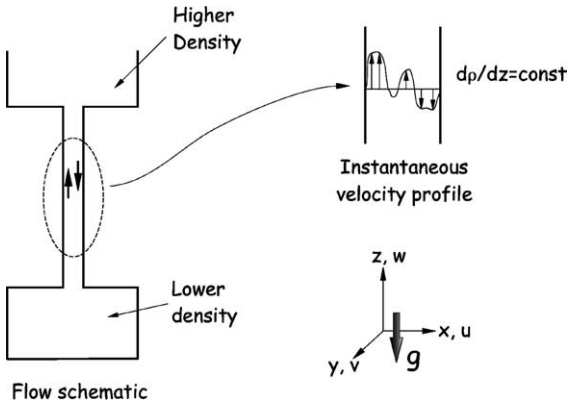

Fig. 1. Flow schematic, and a typical instantaneous axial velocity profile. The axial velocity averages to zero over the cross section at any given instant. The averages at any point over time of the velocities are zero as well.

projecting into the enclosures. The L/d ratios of the tubes were in the range 0.01–10. With a single opening, four different flow regimes were identified as L/d and $\Delta\rho$ were changed: a regime where an oscillatory exchange flow takes place which could be approximately explained by a linearized Taylor-wave theory (regime I), a Bernoulli flow regime where the dynamics is well explained by an inviscid exchange flow model by the application of the Bernoulli theorem [3] (regime II), and at the largest L/d ratios the exchange can be explained by turbulent diffusion, after Gardener [4] (regime IV). The combined effects of turbulent diffusion and Bernoulli flow are observed in regime III, which is modeled as Bernoulli type of flow at the ends of the tube and as a turbulent diffusion at the center of the tube. The peak mixing rate occurs in regime III. A different behaviour at each opening was observed when multiple openings were present. The analysis of this paper covers regimes III and IV.

Arakeri et al. [5] have studied the exchange flow in vertical pipes. The flow is driven by density difference across the pipe created using brine and fresh water. In different experiments, various combinations of pipe diameter and length are used to get a range of Rayleigh number $Ra = g(\Delta\rho/\rho_0 L)d^4/\nu\alpha$ from about 10^5 to 10^8. Using flow visualization, they identified four types of flow as a function of the Rayleigh number. At low Rayleigh numbers the flow is laminar, half-and-half (up and down flowing fluids are side by side). As the Rayleigh number is increased, a helical structure is observed, with the up and down-flowing fluids now forming a double helix. At still higher Rayleigh numbers the flow becomes unsteady, but still remains laminar. Finally beyond about $Ra = 10^7$, the flow was seen to be turbulent with a range of scales. They measured the average salt concentration in the top tank as a function of time and related the rate of change of the average concentration to the average flux of the salt in the pipe. For the turbulent flow, they developed a mixing length model with the length as the diameter of the pipe. In the turbulent case, the measured flux scaled like $\Delta\rho^{3/2}$ as predicted by the model. The laminar flux was higher than the turbulent flux. The convoluted paths in the turbulent flow taken by the fluids from either tank while flowing past each other and the mixing results in the lower flux in the turbulent case.

In the present study, we consider only the turbulent exchange flow which occurs at $Ra > 1 \times 10^8$. We concentrate on flux scaling for the exchange turbulent flow in large AR vertical pipes; the detailed structure of the turbulence is described in Cholemari [6]. We include in the analysis the effects of the developing flow at the pipe ends. We report experiments measuring both the density and the velocity fluctuations.

The aspect ratio AR (length-to-diameter ratio, L/d) of the tube was between 9 and 12. We used brine and distilled water for creating the density difference. The ratio of the diffusivities of momentum and salt, given by the Schmidt number, $Sc = \nu/\alpha$, is about 670, with ν and α being the kinematic viscosity of water and the diffusivity of salt respectively. The Rayleigh number, $Ra = g(\Delta\rho/\rho_0 L)d^4/\nu\alpha$, was of the order of 10^8, where $\Delta\rho$ is the density difference between the top and the bottom tanks, ρ_0 is the density of water and g is the acceleration due to gravity. This definition of Ra involving L and d is appropriate for this problem.

For the turbulent flow we found that the time means of the axial and lateral components of the velocities at each point were zero [6]. Thus there is no mean flow and no mean shear which implies that turbulence production is only due to buoyancy and none due to shear. Away from the ends of the pipe the turbulence was fully developed, or homogeneous in the axial direction. In particular, it can be shown that in the fully developed region the gradient of density is linear. The flow is driven by a linear unstable density gradient.

The rest of the paper is organized as follows. In Section 2 we describe the experiments conducted. Next (Section 3) we describe the modeling of the turbulence using the mixing length type arguments. Using experimental data we then extend the model to include the effects of the ends, and determine the prefactor in case of the flux scaling. We discuss the flow in relation with the Rayleigh–Bénard convection and conclude.

2. Experiments

Experiments were done to produce turbulent convection in long vertical glass pipes, and measure the flow characteristics. We visualized the flow and measured the velocities in the mid-section of the pipe, and the overall flux of salt within the pipe.

The setup (Fig. 2) essentially was a 50 mm diameter glass pipe connecting two tanks TT (Top) and BT (Bottom). The flow is visualized through a rectangular water filled glass tank surrounding the pipe to minimize refraction errors. To prevent stratification in the tanks, the fluid in each tank is continuously mixed. A small aquarium pump P circulated the fluid in each tank; heavier fluid was withdrawn from the bottom of the tank and re-introduced near the top of the tank through perforated pipes (PP). The fluid coming out of PP mixes with the surrounding fluid as it flows down, preventing stratification with minimal disturbance to the flow. The continuous mixing of fluids in the two tanks gives a well defined boundary condition at the two pipe ends.

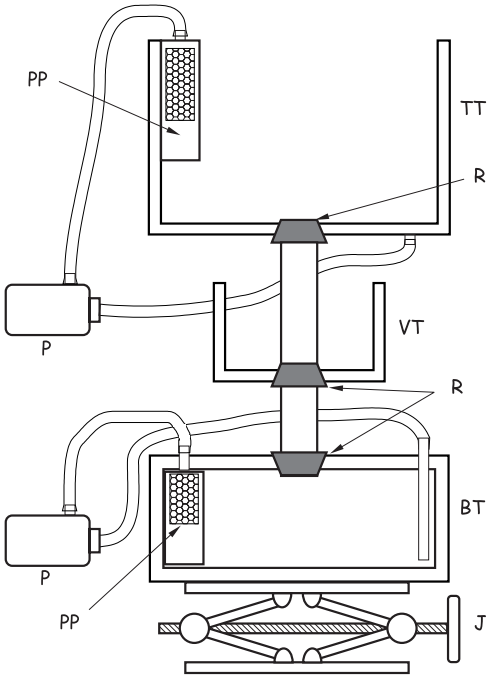

Fig. 2. Schematic of the experimental set-up; see text for notation.

Initially the top tank contains brine while the bottom tank and the pipe contain distilled water. A stopper separates the two fluids; the experiment is initiated by removing the stopper. Once the experiment is started, the fluids from the two tanks mix due to the flow in the pipe, continuously reducing the density difference. The flow thus slowly decays. Typical experiments lasted about three hours, but the flow was turbulent only for about the first 100 min. In our experiments the values of Ra varied from 5×10^8 down to 5×10^7. However the flow was turbulent for Ra larger than 1×10^8. The data considered for this paper is from the turbulent regime.

The flow visualizations (Fig. 3) indicate the flow to be random and three dimensional, with a high rate of mixing. The flow images are from the central homogeneous region, and are visualized with a 1.4 mm thick laser sheet. The process within the pipe is one of overturning and mixing and there is no mean flow. As mentioned above, the mean shear is thus negligible and buoyancy is the only source of turbulent kinetic energy. The pipe wall just contains the flow and has no role in the production of turbulence. The images also show the flow

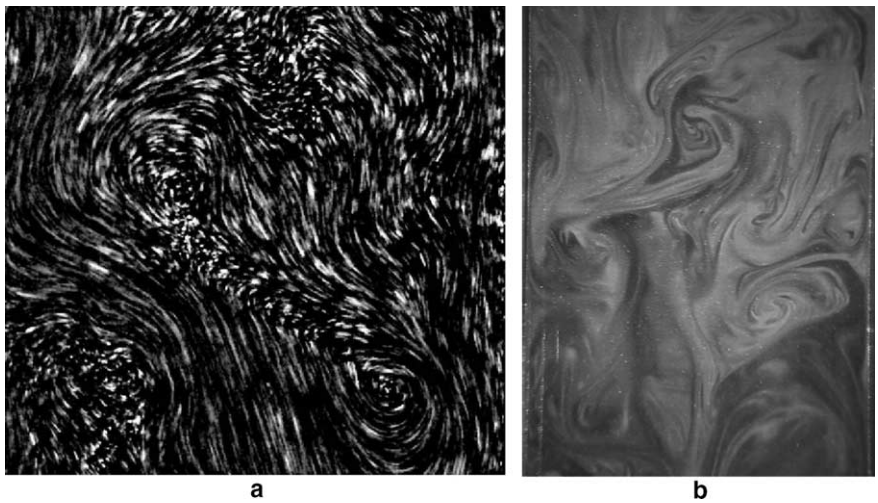

Fig. 3. (a) Particle streak image at $Ra\sim2.5\times10^8$ and (b) Fluorescence dye visualization at $Ra\sim1\times10^8$. The images show the flow to be random and to consist of a range of velocity scales (as seen in a range of streak lengths in (a)) and concentration scales (shown by the variation of image brightness in (b)). The area visualized is 50 mm × 50 mm in (a) and 50 mm × 67 mm in (b). The pipe is vertical in the images.

Table 1
Specifications of diagnostics used in the experiments

Technique	Spatial results	Temporal results	Dynamic range	Error
PIV	1.6/3.2 mm[a]	1 s	1–50 mm/s	~0.5 mm/s
Probe	NA	40 s	1.2–13.3 g/l	0.1% FSD

[a] 1.6 mm with 50% overlap.

to consist of a range of velocity and concentration scales.

We measured velocities at the middle of the pipe in the axial plane using planar Particle Image Velocimetry (PIV) and the salt concentration in the top tank using a conductivity probe (ORION SENSORLINK, model PCM100). Pipes of aspect ratios 9, 12 and 15 were used in the salt concentration experiments, while the velocity measurements were done with the $AR = 9$ pipe. The initial concentration of salt in the top tank was always 10 kg/m^3, corresponding to an Atwood number $At = (\rho_T - \rho_B)/(\rho_T + \rho_B) = 0.0035$. Table 1 gives the summary of the diagnostics. The details of the experiments are in Cholemari [6].

Knowing the rate of variation with time of the salt concentration in the top tank, we can calculate the concentration difference ΔC and the flux of the salt concentration F using an integral balance of the mass of the salt within the pipe;

$$C_B(t) = \frac{M_S - C_T(t)(V_T + V_P/2)}{V_P/2 + V_B} \tag{1}$$

$$\Delta C(t) = C_T - C_B = \frac{C_T(t)(V_T + V_B + V_P) - M_S}{V_P/2 + V_B} \tag{2}$$

$$F = \rho_0 V_T \, dC_T/dt \tag{3}$$

In the above, C_T and C_B are the top and bottom tank concentrations and ΔC the concentration difference; V_T, V_B and V_P refer to the volumes of the top and bottom tanks and the pipe, respectively; A_P is the cross sectional area of the pipe and M_S is the total mass of the salt in the set up. The concentrations are related to the density by,

$$\frac{\partial \rho}{\partial C} = \rho_0 \beta$$
$$\Delta\rho = \rho_0 \beta \Delta C$$
$$\rho = \rho_0 + \Delta\rho = \rho_0 + \rho_0 \beta \Delta C \tag{4}$$

where ρ_0 is the density of water and $\beta = 0.72$ for the salt concentration range encountered in the experiments. $\Delta\rho$ is the density difference between the top and bottom tank fluids.

Fig. 4 gives the flux of salt against the concentration difference. The inset gives the variation with time of the average top tank concentration. It is seen that the overall variation of the flow is slow. Typically an experiment lasts for about 100 min. The flow could thus be considered quasi-steady for periods of a few minutes.

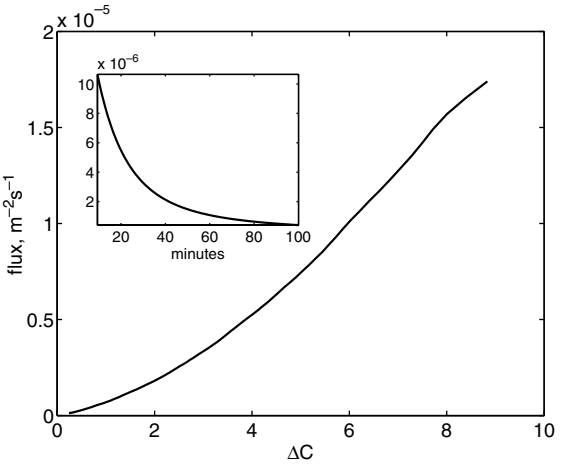

Fig. 4. Plot of the measured salt flux versus the salt concentration difference. Flux versus time is shown in the inset.

3. Model

We now show that the fully developed turbulence in the central region can be described in terms of a single length scale, the diameter of the pipe. The flux of salt, the fluctuations of velocity and the salt concentration are given by this description to within prefactors. The flow at the pipe ends is expected to be different. We extend the mixing length arguments to include the end effects. This enables us to obtain the prefactor in the flux relation as well as to give a relation for the salt flux in terms of the aspect ratio, the overall density difference between the two tanks and the pipe diameter.

For a long enough pipe ($L/d \gg 1$), away from the two ends the flow must be homogeneous in the axial direction with a linear density gradient. The present flow may be compared with the fully developed pressure driven pipe flow. In the latter, the flow is homogeneous (away from the entrance) in the axial direction and driven by a linear pressure gradient; in the present flow, the homogeneous flow is driven by a linear (unstable) density gradient.

First we consider the central homogeneous region. The only relevant parameters are the pipe diameter, d, the density gradient, $d\rho/dz$, g, ν and α. The two molecular parameters ν and α are not relevant for a turbulent flow. Then dimensional analysis gives the scales for density fluctuations ρ', velocity fluctuations w' and salt flux $-\alpha \frac{\partial C}{\partial z} - \langle wc \rangle \simeq -\langle wc \rangle$ as

$$w' \sim \sqrt{g(\partial\rho/\partial z)d^2/\rho_0} = w_m \tag{5}$$

$$\rho' \sim (\partial\rho/\partial z)d = \rho_m \tag{6}$$

$$\frac{w_m\rho_m}{\beta\rho_0} = F_m \tag{7}$$

where w_m, ρ_m and F_m are the mixing length scalings for the fluctuations of velocity and density and the flux of salt respectively. Thus we may write the flux F as

$$F = C_m F_m = C_m \frac{\sqrt{g/\rho_0}(\partial\rho/\partial z)^{3/2}d^2}{\beta\rho_0}. \tag{8}$$

The constant C_m needs to be determined from the experiments.

Physically, the scales may be interpreted as follows. A coherent region of fluid (a fluid particle) scales with the pipe diameter in the fully developed region. The velocity scale can be can be thought as a 'free fall' velocity of the fluid particle heavier (or lighter) than the surrounding fluid by an amount ρ' falling (or rising) through a distance d, i.e., the length over which the correlation exists.

There would be a development region near the pipe ends with non-linear density gradient (Fig. 5) where the distance from the pipe ends would become important in addition to the pipe diameter. Because of the non-linear density gradient, the (unknown) linear density gradient at the central region would be different from $\Delta\rho/L$ (i.e., $\partial\rho/\partial z \neq \Delta\rho/L$).

The parameters relevant to the end regions are L_e, the extent of end region, and $\Delta\rho_e$, the density drop at the ends (see Fig. 5). For a turbulent flow these parameters depend only on the flux and the diameter, as the molecular parameters are not important. The flux is the same throughout the pipe. From (8) we see that flux depends on $(\partial\rho/\partial z)$ and d. Thus $\Delta\rho_e$ and L_e are the functions of the parameters at the central region, viz. $\partial\rho/\partial z$ and d. Thus, from dimensional analysis

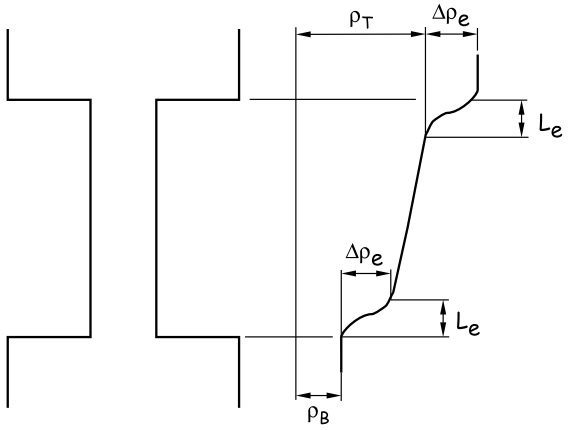

Fig. 5. Schematic of the end regions. The density drops by $\Delta\rho_e$ over a distance L_e. The density variation is non-linear.

$$\Delta\rho_e = k_\rho \frac{\partial\rho}{\partial z} d,$$

$$L_e = k_L d. \tag{9}$$

Thus,

$$\frac{\frac{\partial\rho}{\partial z}}{\Delta\rho/L} = \left(\frac{1-2L_e/L}{1-2\Delta\rho_e/\Delta\rho}\right) = \frac{1}{1+2(k_\rho - k_L)/AR}. \tag{10}$$

The flux is then given by

$$F = C_m \frac{(g/\rho_0)^{1/2}d^2}{\beta\rho_0}\left(\frac{\partial\rho}{\partial z}\right)^{3/2} = C_r \frac{(g/\rho_0)^{1/2}d^2}{\beta\rho_0}\left(\frac{\Delta\rho}{L}\right)^{3/2}, \tag{11}$$

with,

$$C_r = \frac{C_m}{\left(1+2(k_\rho - k_L)/AR\right)^{3/2}}. \tag{12}$$

In the limit of large AR, the entry regions become negligible in comparison with the length of the tube and $C_r \to C_m$. Fig. 6(a) shows the experimentally obtained values of C_r in the experiments of [1,5,7]. Also shown is the fit for the data for $AR > 3$, where a fully developed region is expected to exist at the center, shown as filled symbols. The fit constants are

$$C_m = 0.88 \tag{13}$$

and

$$k_\rho - k_L = 2.1. \tag{14}$$

With these values, (12) becomes,

$$C_r = \frac{0.88}{(1+4.2/AR)^{3/2}}. \tag{15}$$

The fit extended towards smaller AR is shown as the dashed line. It compares quite well with the experimental data even at small AR where the assumption of the existence of a central homogeneous region will not be valid. Velocity measurements near the ends indicate that there is a development region of about one diameter and so we can take $k_L = 1$ which implies $k_\rho = 3.1$, which means that the density drop at the pipe ends is about three times the density drop over one diameter length in the central region. The presence of the end regions reduces the linear density gradient in the centre of the pipe and hence the flux. It follows from Eqs. (9) and (10)

$$\frac{\Delta\rho_e}{\Delta\rho} = \frac{k_\rho}{AR + 2(k_\rho - k_L)}, \qquad \frac{L_e}{L} = \frac{k_L}{AR} \tag{16}$$

These parameters are plotted in Fig. 6(b). It is seen that by about $AR = 10$, the end regions extend only to about 10% of the pipe length at each end, but they account for about 40% of the total density drop across the pipe. These reduce to respectively 5% and 25% by $AR = 20$.

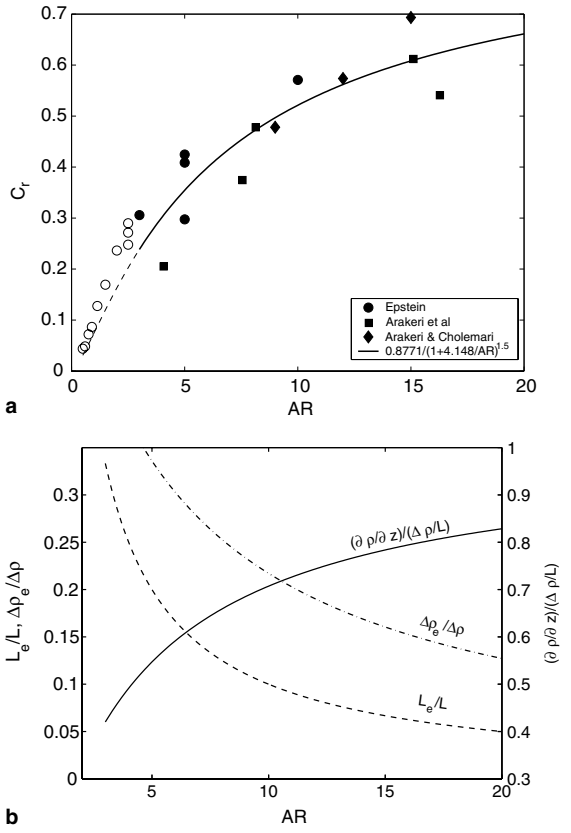

Fig. 6. (a) C_r from experiments (filled symbols), and the model fit (shown as solid line) against the aspect ratio L/d. The dashed line is the extension below $L/d = 3$ (clear symbols). (b) End effects calculated according to the model. Shown are the fraction of the total concentration drop occurring at either end ($\Delta\rho_e/\Delta\rho$) as well as the extent of the region (L_e/L).

C_m, the mixing length prefactor, is expected to be independent of the specific conditions of the flow, like AR, $\Delta\rho/\rho_0$, etc., and is expected to hold when the conditions of a single length scale and the linear density gradient are met.

To compare Eq. (15) with the results of Epstein [1], we note that, Eq. (22) in that paper, when written similar to Eq. (11), shows

$$C_{r'} = \frac{4/\pi \times 0.093}{\left[AR^{-3} + 0.084(1 - 0.4/AR)^3\right]^{1/2}}. \tag{17}$$

The mixing length prefactor calculated from (17) in the limit of large AR, $C_{r'} \to C_{m'} = 4/\pi(0.093/\sqrt{0.084}) = 0.41$. We surmise that the data leading to Eq. (22) in Epstein consists in part of non-turbulent data, leading to the deviation from (13).

The flux relation (11) written in terms of the Nusselt number (the non-dimensional flux), and the Reynolds number using w' ($\sim w_m$) and d have the following scalings with the Rayleigh number:

$$Nu = -\frac{< flux >}{\alpha\Delta C/L} = C_r Ra^{1/2} Sc^{1/2}, \tag{18}$$

$$Re = \frac{w'd}{\nu} \sim Ra^{1/2} Sc^{-1/2}. \tag{19}$$

Note also that $Nu \to C_m Ra^{1/2} Sc^{1/2}$ for very large AR, which is another way of looking at Eq. (18) when the Nusselt number is defined using the density difference over a certain length say, one diameter, in the linear gradient region.

Fig. 7(a) compares the rms velocities obtained from PIV measurements to the velocity scale obtained from

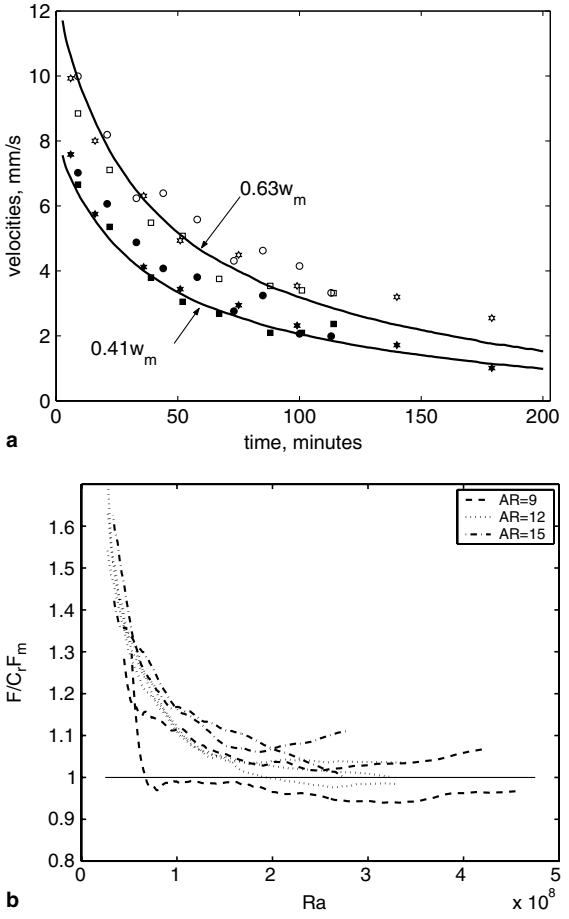

Fig. 7. (a) Velocity scaling according to the mixing length model (lines), compared with the measured velocities (filled symbols—lateral velocity, open symbols—axial velocity). (b) Flux of salt normalized with the flux according to the mixing length model, C_rF_m. The constant regions during the experiments shows the validity of the hypothesis. The pipe diameter is 50 mm.

the model using the density measurements (Eqs. (5) and (4)) in the top tank. Here the average of the RMS velocity calculated over every 10 min over the pipe cross section area is plotted with time. It is seen that the scaling is good for the regime under consideration, both the axial and lateral velocities following the mixing length scaling w_m. However beyond about 100 min when the flow is no longer turbulent, the agreement is poor. Fig. 7(b) shows the turbulent flux normalized with the flux obtained from the model (Eq. (11)). The value is constant and within 10% of unity for an extended range of the Rayleigh number. However, at lower Rayleigh numbers below 1×10^8, the turbulent scaling is not appropriate and the normalized fluxes rise sharply above unity. The flow is not turbulent for $Ra < 2 \times 10^8$.

The overall uncertainty in the measured flux scaling is obtained from Eq. (8) as

$$\frac{\epsilon_F}{F} = \frac{3}{2}\frac{\epsilon_{\Delta\rho}}{\Delta\rho}. \tag{20}$$

The worst case is at the smallest density differences, where the error is about 1.5% (see Table 1).

The Nusselt number relation (18) is of the same form as the theoretical expression of Kraichnan [8], for Rayleigh–Bénard (R–B) convection at very high Rayleigh numbers of the order of 10^{18}, where the flow mechanics is expected to be dominated by the processes in the bulk of the flow, away from the walls. However, no experimental evidence for the $Ra^{1/2}$ regime is seen in R–B convection, even at very high Rayleigh numbers of about 10^{17} achieved so far in the experiments [9]. An important difference between the two types of flows is that, in R–B convection, even at high Rayleigh numbers, boundary layers exist near the two horizontal walls and have an effect on the flow, whereas in the present flow boundary layers are absent.

It can be shown that the flux obtained for a given density difference in the present flow is much higher than the flux in R–B convection at the same density difference. To do this, we first obtain the prefactor in Eq. (18) to be 0.0752 at unit aspect ratio (as we want to compare with R–B convection which is at about unit aspect ratio or lower) using Eq. (12). Nusselt number at $Ra = 10^8$ and $Sc = 670$ then turns out to be ~1950. To obtain a similar estimate in case of R–B convection, we use the experimental correlation of Globe and Dropkin [10], $Nu \sim 0.097 Ra^{1/3}$. This is for a Prandtl number of 100, but we assume its validity for $Pr = 670$ and estimate the Nusselt number at the same Rayleigh number to be much smaller, ~45.

4. Conclusion

In this paper we have described a purely buoyancy driven turbulent flow in long vertical pipes, with a fully developed region of turbulence with an unstable linear density gradient. Using a mixing length theory and dimensional arguments, we have developed a relation for the flux in the present turbulent convection. The analysis includes the effects of the ends. Experimental results have been used to validate the predicted scaling and to obtain values of the constants in the flux relations. Eq. (11) with C_r determined empirically in (15) is the relation for the flux. The flux is a function of the concentration difference, the pipe length and the aspect ratio. The scaling relations for the velocity fluctuations are well predicted by the model (Eq. (5) and Fig. 7(a)). This is of use in design practice, for example, when air fluxes need to be calculated across a staircase connecting rooms with different temperatures.

The mixing length model implies the Nusselt number to scale as $\sim Ra^{1/2}$, in contrast to R–B convection for similar Rayleigh numbers as in the present flow, where it goes like $\sim Ra^n$, with $2/7 < n < 1/3$. The absence of the top and bottom horizontal walls and the associated boundary layers in the present flow mainly accounts for this large difference.

References

[1] M. Epstein, Buoyancy driven exchange flow through small openings in horizontal partitions, J. Heat Transfer 110 (1988) 885–893.
[2] Q. Tan, Y. Jaluria, Mass flow through a horizontal vent in an enclosure due to pressure and density differences, Int J. Heat Mass Transfer 44 (2001) 1543–1553.
[3] W.G. Brown, Natural convection through rectangular openings in partitions—2: horizontal partitions, Int. J. Heat Mass Transfer 5 (1962) 869–881.
[4] G.C. Gardener, Motion of miscible and immiscible fluids in closed horizontal and vertical ducts, Int. J. Multiphase Flow 3 (1977) 305–318.
[5] J.H. Arakeri, F.E. Avila, J.M. Dada, R.O. Tovar, Convection in a long vertical tube due to unstable stratification—a new type of turbulent flow? Current Sci. 79 (6) (2000) 859–866.
[6] M.R. Cholemari, Buoyancy driven turbulence in a vertical pipe, Ph.D. thesis, Department of mechanical engineering, Indian Institute of Science, 2004.
[7] J.H. Arakeri, M.R. Cholemari, Fully developed buoyancy driven turbulence in a tube, in: Proceedings of the 9th Asian Congress Fluid Mech., Isfahan University of Tech., Iran, 2002.
[8] R.H. Kraichnan, Turbulent thermal convection at arbitrary Prandtl number, Phys. Fluids 5 (11) (1962) 1374–1389.
[9] J.J. Niemela, L. Skrbek, K.R. Sreenivasan, R.J. Donnelly, Turbulent convection at high Rayleigh numbers, Nature 404 (2000) 837–841.
[10] S. Globe, D. Dropkin, Natural convection heat transfer in liquids confined by two horizontal plates and heated from below, ASME J. Heat Transfer 81 (1959) 24–28.